Verification of Calculation Methods for Unsteady Airloads in the Prediction of Transonic Flutter

R. J. Zwaan*
National Aerospace Laboratory (NLR), Amsterdam, the Netherlands

Various engineering-type methods to calculate unsteady airloads on wings in transonic flow were applied in flutter calculations for a semispan flutter model of a supercritical wing. Verification was performed on the basis of comparing flutter characteristics, in which special attention was given to the prediction of transonic dips in the flutter boundaries. The methods were able to produce useful results when applied complementarily.

Nomenclature

b = dimensionless shift of aerodynamic center
c = wing section chord, m
C_{l_0} = sectional mean lift coefficient
$C_{P_{0.95}}$ = pressure coefficient at 0.95 chord, 0.7 span, upper side
f = frequency, Hz
k = reduced frequency related to semichord
k_α, m_α = sectional unsteady lift and moment coefficients (AGARD notation, m related to 0.25 chord); $k_\alpha = k'_\alpha + ik''_\alpha$, $m_\alpha = m'_\alpha + im''_\alpha$
k_{ij}, m_{ij} = sectional unsteady lift and moment influence coefficients (induced by strip j, at strip i)
M_∞ = Mach number
P_0 = stagnation pressure, kPa
s = flutter model span, $s = 0.635$ m from tunnel wall
α_0 = mean wing angle of incidence, deg

Superscripts

DL = doublet-lattice
EXP = experiment
T = transonic

Subscripts

a = heaving motion
b = pitching motion about 0.25 chord
e = equivalent
F = flutter boundary
i,j = wing strip index
2D,3D = two- and three-dimensional
α = arbitrary motion

I. Introduction

An extensive flutter investigation was completed recently at NLR, including wind tunnel tests of a semispan supercritical wing model and flutter calculations based on different approaches to modeling unsteady airloads on the wing. The aim of this investigation was to explore the transonic flutter characteristics of an advanced transport aircraft, especially the transonic dip in the flutter boundary, and to evaluate calculation methods for unsteady transonic airloads that could be used in the preliminary design stage.[1] The first flutter test was carried out in 1979.[2] Although instructive, the test was not totally successful, mainly because of unexpected instabilities at low Reynolds numbers which prevented the measurement of complete transonic dips. The second flutter test followed in 1982.[3] The model was slightly modified—in one wing section a number of pressure orifices were installed in the wing upper surface to monitor the mean flowfield, especially shock position and flow separation, and a transonic strip of larger roughness was applied to guarantee transition also at low Reynolds numbers. This test was successful to a high degree. The last part of the investigation—evaluation of methods to calculate the unsteady transonic airloads to be used during the aircraft design and the analysis of the flutter test results—forms the subject of the present paper.

II. Outline of Flutter Model Tests

The flutter model shown in Fig. 1. was attached to a turntable through an instrumented torsional spring in the wind tunnel side wall. The model did not simulate the aeroelastic characteristics of any full-scale aircraft design in that the wing itself was relatively stiff.

The flutter characteristics were controlled by a spring designed to enable flutter instabilities within the operational limits of the wind tunnel. Model excitation was provided most times by residual turbulence in the flow. Two shakers were installed to be used either as alternative forced excitation or as flutter dampers in case of turbulence excitation to enable flutter testing at neutral stability and even slightly beyond the flutter boundary. Model responses were measured by strain-gage bridges on the spring and accelerometers in the mode. In the second flutter test the mean pressure distribution on the wing upper side also could be measured in a section at 0.7 wing span. By correlating these pressures with results of earlier steady pressure tests with a model that had six measuring sections along the span, detailed knowledge was available. This knowledge was required to determine the unsteady airloads for the flutter calculations. Since the pressure and flutter models had the same geometry and structure, the mean deflections of the wing were nearly the same, which could be confirmed afterward by comparing the combinations of mean angle of incidence at the wing root and mean pressure distribution at 0.7 wing span. The two vibration modes, measured at zero flow speed, and acting as degrees of freedom in the flutter analysis, could be characterized by wing bending (mode 1) and wing rotation about the spring axis (mode 2). The mode shapes are shown in Fig. 2. Vibration modes with higher frequencies were not considered as the next higher frequency was only at about 210 Hz (overtone bending).

Presented as Paper 84-0871 at the AIAA/ASME/ASCE/AHS 25th Structures, Structural Dynamics and Materials Conference, Palm Springs, CA, May 14-16, 1984; received July 9, 1984; revision received April 22, 1985.

*Head, Department of Aeroelasticity.

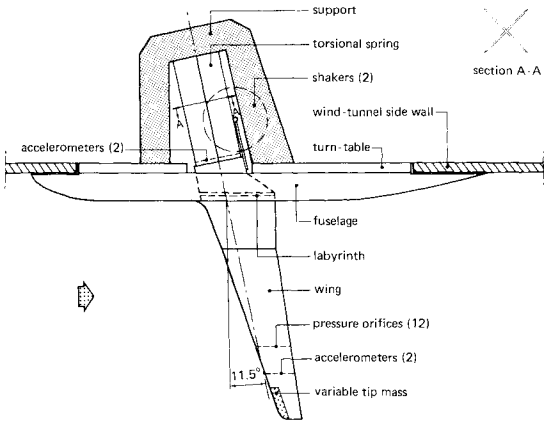

Fig. 1 Global view of flutter model and support.

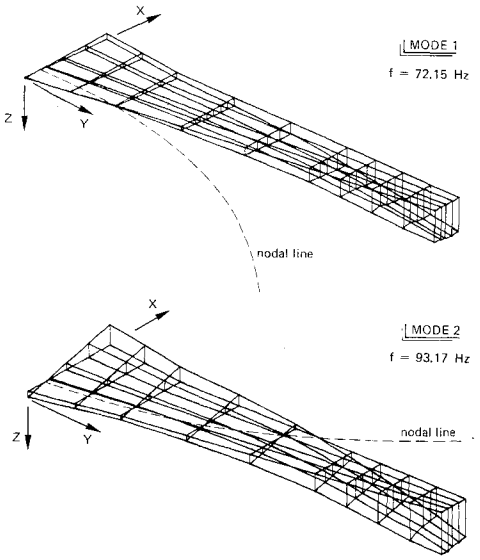

Fig. 2 Vibration modes of the wing model.

A survey of the results of the second flutter test is presented in Fig. 3. At the top the flutter boundaries $P_{0_F}(M_\infty)$ are shown for three wing incidence angles α_0, obtained by increasing the total pressure at constant Mach number and vice versa. Complete transonic dips were measured which shifted to lower Mach numbers at higher wing incidence angles. At the highest value even two dips were found. Comparison with the flutter frequency curves $f_F(M_\infty)$ (Fig. 3, middle) shows that primarily mode 1 participated in the flutter mode, whereas in the second dip at the highest wing incidence the flutter mode was almost identical with mode 2.

Comparison with the pressure $C_{P_{0.95}}$ near the trailing edge on the upper surface of the pressure section (Fig. 3, bottom) shows that the dips correspond to predominantly attached flow, except for the second dip which appeared very clearly in separated flow. The latter type of flutter may be identified with wing torsional buzz.[4]

III. Survey of Applied Unsteady Transonic Airload Methods

The following methods were used in the flutter analysis to calculate the unsteady airloads.

1) DL: A conventional three-dimensional subsonic doublet-lattice method, applied as reference.

2) DL + QS: A widely used method consisting of DL with quasisteady transonic corrections derived from the three-dimensional steady pressure model tests mentioned in Sec. II.

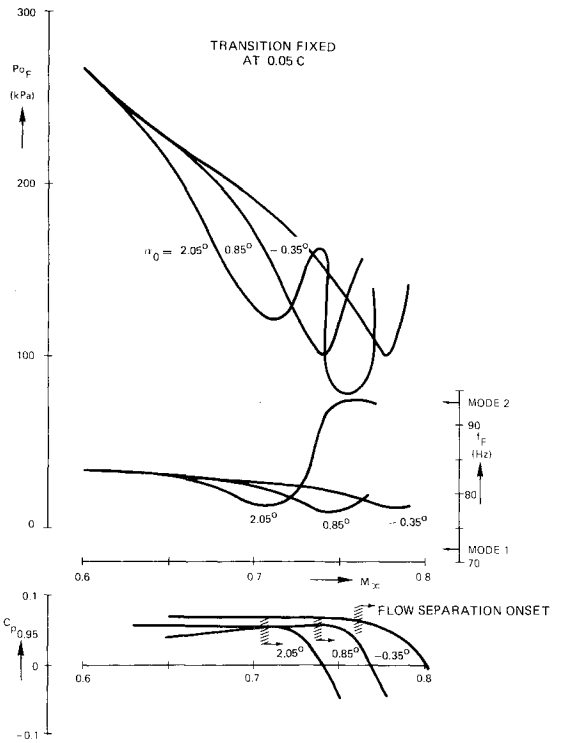

Fig. 3 Results of the second wind tunnel flutter test.

3) Q3D + LTRAN2NLR: A quasi-three-dimensional method for wings of large aspect ratio, based on a) the two-dimensional code LTRAN2 in its moderate reduced frequency version developed at NLR, and b) finite span corrections obtained from two- and three-dimensional DL. This method was to be evaluated primarily as it was intended for use afterward in the aircraft preliminary design stage.

4) Q3 + 2DEXPT: Similar to the previous method except for the LTRAN2 values being replaced by experimental data derived from two-dimensional unsteady pressure tests.

5) EQS: The so-called "extended quasisteady" method, which combines quasisteady spanwise load distributions obtained from the steady tests mentioned in Sec. II and unsteady two-dimensional airloads derived from the unsteady tests mentioned under method 4. This method was developed to predict flutter characteristics for separated flow.

6) FTRAN3: A very recent field panel/finite difference method for three-dimensional potential unsteady transonic Q3D + LTRAN2NLR.

In the following, brief explanations of these methods are given together with the results of their application in the flutter calculations. These calculations were performed using the well-known *p-k* method.

IV. Verification of Unsteady Transonic Airload Methods

DL + QS

The quasisteady corrections in DL + QS were defined as follows. Correction factors were derived from matching the quasisteady spanwise lift and moment distributions calculated with DL to the experimental values obtained from the steady pressure model tests mentioned in Sec. II. These factors were applied to the unsteady lift and moment coefficients for arbitrary motion α and reduced frequency k, as follows:

$$k_\alpha(k) = [k_b^{\mathrm{EXP}}(0)/k_b^{\mathrm{DL}}(0)]\, k_\alpha^{\mathrm{DL}}(k) \tag{1}$$

$$m_\alpha(k) = [m_\alpha^{\mathrm{DL}}(k) + bk_\alpha^{\mathrm{DL}}(k)]\,[k_b^{\mathrm{EXP}}(0)/k_b^{\mathrm{DL}}(0)] \tag{2}$$

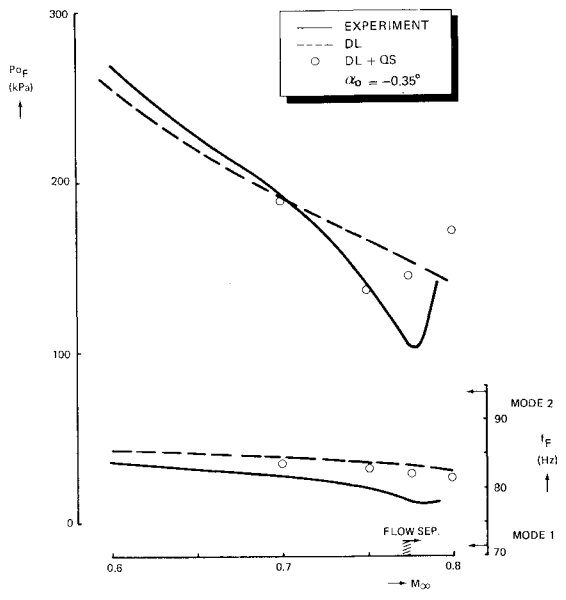

Fig. 4 Flutter results according to DL and DL + QS.

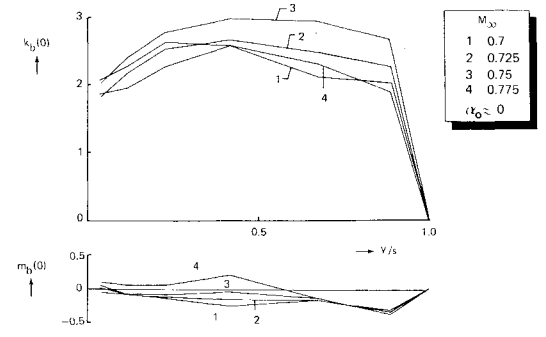

Fig. 5 Spanwise distributions of quasisteady lift and moment coefficients.

with

$$b = m_b^{\mathrm{EXP}}(0)/k_b^{\mathrm{EXP}}(0) - m_b^{DL}(0)/k_b^{\mathrm{DL}}(0) \tag{3}$$

Here b can be interpreted as a shift of the aerodynamic center. Flutter boundaries and frequency curves are presented for the lowest angle of incidence in Fig. 4. The results of DL itself, of course, do not lead to any transonic effect and, therefore, are unconservative. The flutter boundary calculated with DL + QS has indeed a transonic dip, although less descending and at a slightly lower Mach number than the measured boundary. This makes the DL + QS results unconservative at the measured dip. The position of the calculated dip can be correlated with the decrease of $k_b^{\mathrm{EXP}}(0)$ beyond $M_\infty = 0.75$, especially in the tip region, shown in Fig. 5. It is noteworthy that the differences between the calculated and measured flutter boundaries are completely consistent with the results of similar flutter model investigations of the TF-8A[5] and Airbus A 310.[6]

Q3D + LTRAN2NLR and FTRAN3

The main assumption of the Q3D method is that the relation between the unsteady aerodynamic loading in a section of a wing of large aspect ratio and the loading of an equivalent two-dimensional wing with that section is not influenced by transonic effects and can be obtained from subsonic DL theory. An outline of the method is given in Fig. 6. The wing is subdivided into streamwise strips. The three-dimensional DL

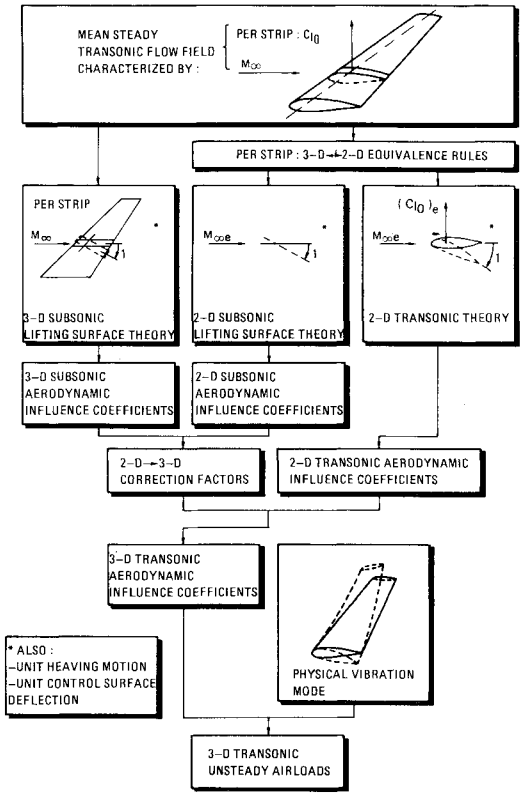

Fig. 6 Outline of the Q3D + LTRAN2NLR method.

method is used to compute lift and moment coefficients for unit pitching and heaving of each strip. The results form a matrix of subsonic three-dimensional aerodynamic influence coefficients. Next, a two-dimensional DL method is used for each strip oscillating in equivalent two-dimensional flow conditions, including local reduced frequency values. The results are put into a diagonal matrix. Analogously the transonic two-dimensional code LTRAN2-NLR is applied. A crucial step then is to select the initial steady flow conditions for the LTRAN2-NLR computation in such a way that the mean pressure distribution, and especially the shock position, fits in with experimental data. This matching procedure is explained further later in this section.

Finally, a matrix of three-dimensional transonic strip influence coefficients for lift and moment can be obtained (both for unit pitching and heaving):

$$k_{ij_{3D}}^T = [k_{ij_{3D}}^{\mathrm{DL}}/k_{jj_{2D}}^{\mathrm{DL}}]\,k_{jj_{2D}}^T \tag{4}$$

$$m_{ij_{3D}}^T = [m_{jj_{2D}}^T + b_{ij}\,k_{jj_{2D}}^T]\,[k_{ij_{3D}}^{\mathrm{DL}}/k_{jj_{2D}}^{\mathrm{DL}}] \tag{5}$$

with

$$b_{ij} = m_{ij_{3D}}^{\mathrm{DL}}/k_{ij_{3D}}^{\mathrm{DL}} - m_{jj_{2D}}^{\mathrm{DL}}/k_{jj_{2D}}^{\mathrm{DL}} \tag{6}$$

b_{ij} may be considered again as a shift of the aerodynamic center. The spanwise load distributions and generalized aerodynamic forces can be calculated when the spanwise variations of pitching and heaving are given.

To reduce computational costs, the transonic flow computations and matching are usually carried out only for one representative wing section rather than for each strip separately. In the present flutter analysis the representative section was chosen at 0.7 wing span, where the pressure orifices were also located. The procedure to match the calculated mean pressure distribution and experimental data is explained in Fig. 7. Use was made again of the results of three-dimensional steady pressure model tests, in which the model deflections

were much the same as the mean model deflections in the flutter test. The elastic nosedown twist angle for that steady pressure model was calculated to be about 0.5 deg at the tip with respect to the root.

Starting with the incidence angle of the flutter model corrected for deformation of the torsional spring, a pressure distribution at $y/s=0.7$ was found that was made to match a mean pressure distribution calculated with LTRAN2-NLR. The corresponding value of the calculated lift coefficient C_l was used to interpolate in tables of previously prepared tables of unsteady coefficients, also calculated by LTRAN2-NLR with M_∞, k, and C_l as parameters. For wing sections other than $y/s=0.7$, the relations valid for $y/s=0.7$ were used.

Results with Q3D + LTRAN2NLR are presented in Figs. 8 and 9. At $\alpha_0=0.05$ deg, Fig. 8, the calculated flutter boundary and frequency curve agree relatively well with the measured data all along the descending part of the transonic dip. The calculated flutter boundary is slightly conservative due to the absence of boundary-layer effects.

The degree of conservatism corresponds to experience from past wind tunnel flutter tests at NLR. The calculation was stopped at $M_\infty=0.775$ where flow separation was about to start, which, of course, could not be taken into account by LTRAN2-NLR.

At $\alpha_0=2.05$ deg, Fig. 9, the calculated flutter boundary has become unconservative, most probably being caused by violation of the small-perturbation concept of LTRAN2-NLR at this angle of incidence. An improvement is foreseen when the development of a two-dimensional full-potential code has been finished at NLR.[7]

It is striking that in both cases only the descending parts of the transonic dip are predicted, but no complete dips. This can be explained as follows. In the experimental transonic dip the flow separation prevents the shock wave from moving further downstream with increasing Mach number, and causes a drastic change in unsteady airloads and, correspondingly, a sudden increase of the flutter boundary. Of course, this cannot be predicted by the present inviscid theory. In the absence of flow separation, the calculated results would show a transonic dip at a Mach number at which the shock wave approaches the trailing edge and the unsteady airloads become supersonic. Such an inviscid type of transonic dip was com-

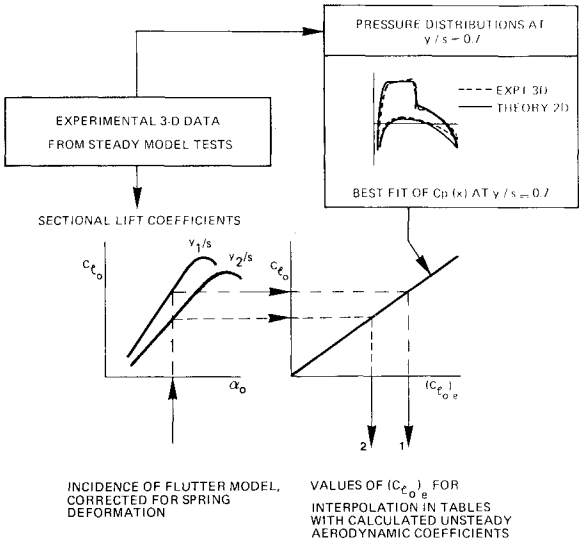

Fig. 7 Determination of $(C_{l_0})_e$ in flutter model wing sections.

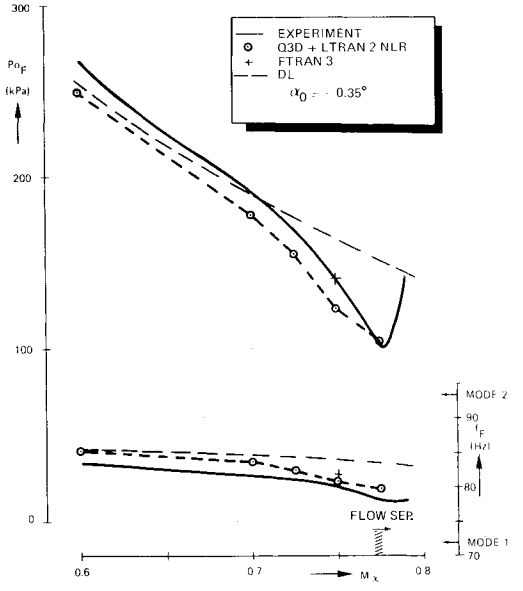

Fig. 8 Flutter results according to experiment and Q3D + LTRAN2NLR.

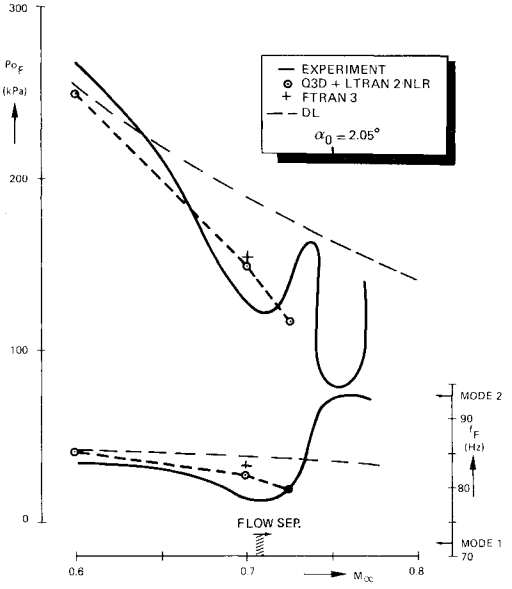

Fig. 9 Flutter results according to experiment and Q3D + LTRAN2NLR.

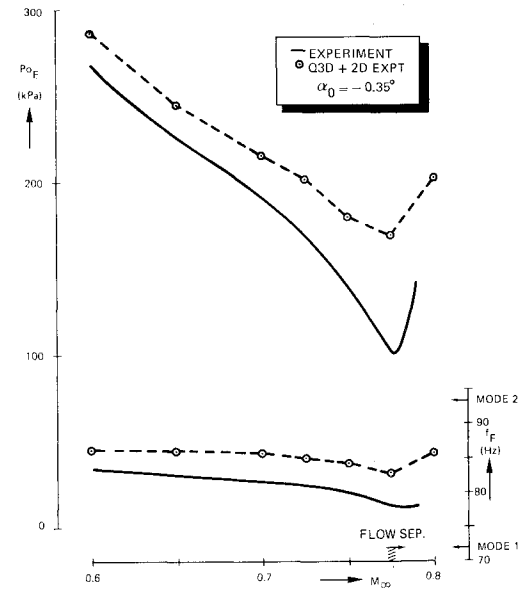

Fig. 10 Flutter results according to experiment and Q3D + 2DEXPT.

puted by Isogai for aeroelastic models of swept wings with supercritical characteristics on the basis of a full-potential theory,[8] later extended with a steady turbulent boundary-layer method.[9] In both cases the transonic dip was influenced by a relatively high mean elastic twist angle (5.5 and 4 deg, respectively, nosedown, with respect to the root). In general, the degree of realism of a predicted transonic dip is confined to those flow conditions for which a proper agreement between the computed and measured mean flowfield about the wing exists.

A new possibility to verify Q3D+LTRAN2NLR was offered recently after the code FTRAN3 for three-dimensional potential unsteady transonic flow was put into use.[10,11] The code is based on a time-linearized finite difference method, embedding a so-called field panel method which accounts properly for the mean flowfield, the shock wave motions, and the radiation of signals toward infinity. The mean flowfield is calculated with the code XFLO22, also developed at NLR, by which steady transonic flow about wings and bodies can be obtained.[12]

In the present case, the mean flowfields, including the effect of mean wing deflections, were tuned with the aid of data from the steady pressure model tests. The FTRAN3 computations were based on $9\times14\times16$ grid points (i.e., spanwise $\times$ normal $\times$ streamwise, with 6×10 on each wing surface). The preliminary results shown in Figs. 8 and 9 do not confirm the correctness of the Q3D+LTRAN2NLR results completely. An analysis of their differences is in progress, which will also include FTRAN3 results using a finer mesh.

Q3D+2DEXPT

As an alternative to the LTRAN2 airloads, experimental data from two-dimensional unsteady pressure tests could also be applied. These data referred to a wind tunnel test of a supercritical airfoil[13] with approximately the same contour as the flutter model pressure section at $y/s=0.7$. Mean steady and unsteady aerodynamic coefficients were obtained for pitching and heaving oscillations, both in attached and separated flow. As the data were available only for a few mean angles of attack, interpolation according to Fig. 7 was omitted and a constant value of $(C_{l_0})_e$ along the span was assumed.

Results with Q3D+2DEXPT are presented in Fig. 10 for $\alpha_0=-0.35$ deg. The two-dimensional experimental airloads data corresponded to $\alpha_0=0$ deg (when corrected for tunnel wall effects, the true α_0 varied between -0.39 and -0.43 deg). Comparison of calculated and measured flutter boundaries and frequency curves shows that a qualitative agreement exists, including a complete transonic dip. The nonconservative margin of the calculated flutter boundary should be ascribed largely, at least for the descending part of the dip, to the unsteady tunnel wall interference effects, which could not be removed as an approved correction procedure for slotted walls is still nonexistent.

For flow conditions with substantial separated flow areas, the aforementioned assumption concerning $(C_{l_0})_e$ is too restrictive and should be released if adequate measured data were available. A less demanding but more global way would be to distinguish parts of the wing span where the flow is either attached or separated and to apply corresponding mean and unsteady measured data. The question remains as to whether the quasi-three-dimensional concept, being based on doublet-lattice-type finite span corrections, could be maintained. For this reason, a still more global approach was taken which made use directly of measured quasisteady spanwise load distributions.

EQS

EQS has been set up as a qualitative method that makes extensive use of measured quasisteady spanwise load distributions in combination with measured two-dimensional unsteady aerodynamic coefficients. The method is intended to

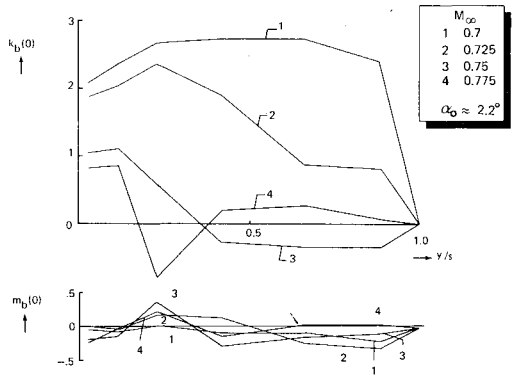

Fig. 11 Spanwise distribution of quasisteady lift and moment coefficients.

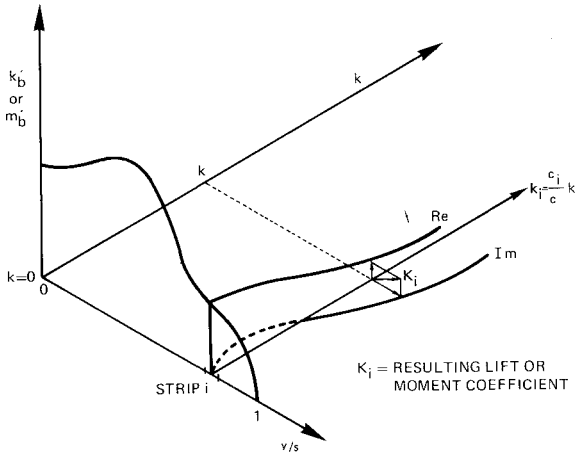

Fig. 12 Principle of EQS method to determine unsteady airloads based on spanwise quasisteady lift k_b and moment m_b distributions.

apply also in separated flow conditions where advanced computational means are not yet available and, as such, the method forms a supplement to the previous methods. As an example of the influence of flow separation, the spanwise distributions of lift and moment coefficients are shown in Fig. 11 for $\alpha_0\approx2.2$ deg. These data were derived from the steady pressure model tests mentioned previously in Sec. II. At $M_\infty=0.7$, no flow separation occurs. An increase to $M_\infty=0.725$ leads to separation onset along the outer part of the wing, being centered at about $y/s=0.7$, while at the same time k_b decreases. The separation has spread along the entire wing span at $M_\infty=0.75$, while at the outer wing k_b has even become negative. At $M_\infty=0.775$ this coefficient is positive again, although small. The moment coefficients indicate that at the same time the aerodynamic center position shifts considerably; at the outer wing first upstream and above $M_\infty=0.725$ downstream.

The principle of EQS is illustrated in Fig. 12. The wing is divided into streamwise strips. In each strip the measured quasisteady coefficients k_b and m_b are extended into the frequency domain by means of the measured two-dimensional unsteady coefficients mentioned in the previous subsection. At $k=0$ these coefficients are scaled to the three-dimensional quasisteady values. For $k>0$ the strip values of the reduced frequency, k_i, are taken into account. The coefficients may correspond to either attached or separated flow.

In Fig. 13 two types of measured two-dimensional lift coefficients k_α (pitching about 0.45 chord) are given as an example: one for attached flow (I) and the other one for separated flow (II), plotted as functions of k and in vector form. At condition I, k_α shows a typical behavior for attached flow. (The

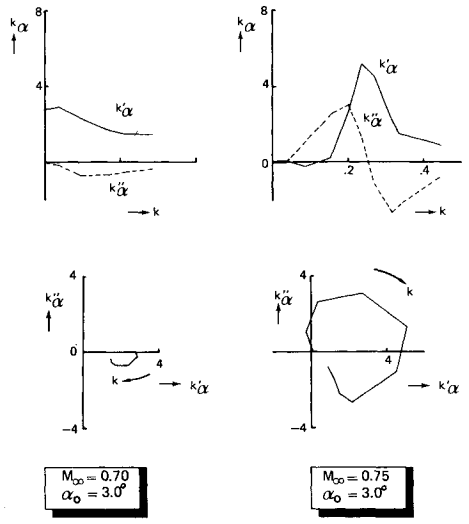

Fig. 13 Measured two-dimensional unsteady lift coefficients for pitching about 0.45 chord.

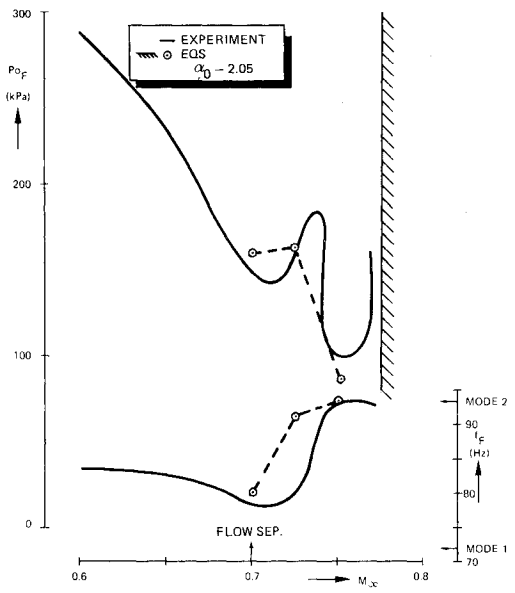

Fig. 14 Flutter results according to experiment and EQS.

anomaly for $k \to 0$ is due to wall interference.) In contrast, at condition II, k_α exhibits enormous phase shifts and almost vanishes at $k \to 0$. This behavior, which was reported to occur both for conventional and supercritical airfoils,[14,15] can be associated with the phenomenon of a reversed shock wave motion (i.e., upstream with increasing angle of attack). In vector form, the coefficient reflects an aerodynamic mechanism being brought into resonance (cf., the well-known circle-type response loops of mechanical systems), which will certainly contribute considerably to the buzz-type instability in the second dip.

Because of the different characteristics of the unsteady coefficients for $k \to 0$ in the two conditions, different scaling procedures were used:

Condition I:

$$k_b(k) = [k_{b_{3D}}(0)/k_{b_{2D}}(0)]\,k_{b_{2D}}(k) \tag{7}$$

$$k_a(k) = [ik\,k_{b_{3D}}(0)/(k_{a_{2D}}/k)_{k=0}]\,(k_{a_{2D}}(k)/k) \tag{8}$$

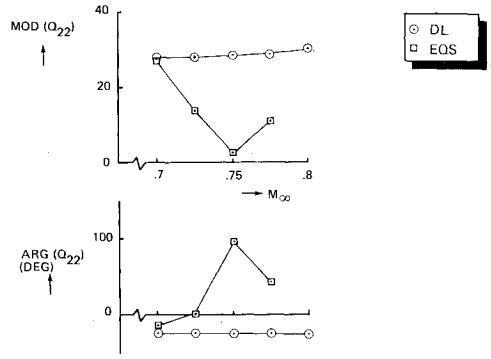

Fig. 15 Calculated generalized aerodynamic force Q_{22} according to DL and EQS (k related to $c_{root}/2 = 0.0965$ m).

Condition II:

$$k_b(k) = k_{b_{2D}}(k) + k_{b_{3D}}(0) - k_{b_{2D}}(0) \tag{9}$$

$$k_a(k) = k_{a_{2D}}(k) + ik\,k_{b_{3D}}(0) \tag{10}$$

The moment coefficients were formulated likewise by replacing k_a and k_b with m_a and m_b.

Results with EQS are presented in Fig. 14 for $\alpha_0 = 2.05$ deg (comparable to the quasisteady spanwise load distribution of 2.2 deg in Fig. 11). The result is that the calculated flutter boundary corresponds fairly well with the measured boundary and that indeed a second dip is predicted, while the frequency curve indicates that the flutter mode can be identified almost completely with mode 2. The relation between the second dip instability and the previously mentioned aerodynamic resonance phenomenon is illustrated in Fig. 15 by the generalized aerodynamic force Q_{22} which is responsible for the second dip. In spite of the small modulus value at $M_\infty = 0.75$, it is the positive phase angle that causes the instability.

VI. Conclusions

A number of engineering-type methods for the calculation of unsteady transonic airloads have been evaluated herein, which can be used to complement the preliminary design stage of modern transport wings. The verification has been performed by comparison with results of a flutter model test. Emphasis is put on the prediction of transonic dips in the flutter boundaries.

1) Applying DL + QS, involving the doublet-lattice method provided with quasisteady corrections obtained from steady model tests, leads to an unconservative prediction of the transonic dip.

2) Application of Q3D + LTRAN2NLR, which combines two-dimensional and three-dimensional doublet-lattice methods with the two-dimensional LTRAN2 code (NLR version), leads to satisfactory predictions at low wing incidence up to the Mach number of flow separation onset. At higher wing incidences the prediction becomes unconservative. Since the transonic dips in this flutter investigation are primarily caused by flow separation, they are not predicted. Preliminary results of FTRAN3, an advanced field panel/finite difference method for three-dimensional potential unsteady transonic flow, do not yet confirm the results of Q3D-LTRAN2NLR.

3) Application of Q3D + 2DEXPT, in which measured two-dimensional unsteady airloads are used, leads to qualitatively correct results, including separation onset. The results are nonconservative due to tunnel wall-interference effects in the measured airload data which could not be removed.

4) Applying EQS, involving measured quasisteady spanwise load distributions and measured two-dimensional unsteady airloads, leads to a fairly good prediction. Especially the second transonic dip is predicted correctly.

5) When applied complementarily, the methods are able to produce a useful prediction of the flutter characteristics, both in attached and separated flow. It is extremely important that the mean flowfield be represented correctly.

Acknowledgments

This investigation was carried out partly under contract with the Netherlands Agency for Aerospace Programs (NIVR) and the Netherlands Department of Civil Aviation (RLD).

Various members of the NLR Department of Aeroelasticity contributed in some way, of which Mr. A. Steiginga (who has left NLR in the interim) should be mentioned as being responsible for the major part of the flutter analysis. In addition, Mr. H. J. Hassig, of Lockheed-California, is acknowledged for his suggestions in formulating the Q3D method.

References

[1]Pronk, N., Walgemoed, H., and Zwaan, R. J., "Transonic Flutter Clearance for a Supercritical Transport Aircraft in the Preliminary Design Stage," AGARD-CP-354, 1983, pp. 5-1 to 5-13.

[2]Houwink, R., Kraan, A. N., and Zwaan, R. J., "A Wind Tunnel Study of the Flutter Characteristics of a Supercritical Wing," *Journal of Aircraft*, Vol. 19, May 1982, pp. 400-405; also, NLR MP 81002 U, Jan. 1981.

[3]Persoon, A. J., Horsten, J. J., and Meijer, J. J., "On Measuring Transonic Dips in the Flutter Boundaries of a Supercritical Wing in the Wind Tunnel," AIAA Paper 83-1031-CP, May 1983; also, NLR MP 83008 U, Jan. 1983.

[4]Moss, G. F. and Pierce, D., "The Dynamic Response of Wings in Torsion at High Subsonic Speeds," AGARD-CP-226, 1977, pp. 4-1 to 4-21.

[5]McGrew, J. A., Giesing, J. P., Pearson, R. M., Zuhuruddin, K., Schmidt, M. E., and Kalman, T. P., "Supercritical Wing Flutter," AFFDL-TR-78-37, March 1978.

[6]Zimmermann, H., "Flight Vibration Testing with Tip Vane on Airbus A310," AIAA Paper 83-2753, Nov. 1983.

[7]Schippers, H., "Numerical Integration of the Unsteady Full-Potential Equation with Applications to Transonic Flow about a 2D Airfoil," NLR MP 84022 U, March 1984.

[8]Isogai, K. and Suetsugu, K., "Numerical Simulation of Transonic Flutter of a Supercritical Wing," NAL TR-726T, Aug. 1982.

[9]Isogai, K., "Numerical Simulation of Transonic Flutter of a High-Aspect-Ratio Transport Wing," NAL TR-776T, Aug. 1983.

[10]Hounjet, M. H. L., "A Hybrid Field Panel/Finite Difference Method for 3-D Potential Unsteady Transonic Flow Calculations," AIAA Paper 83-1690, July 1983; also, NLR MP 83023 U, May 1983.

[11]Hounjet, M. H. L. and van der Kolk, J. T., "Application of NLR's Numerical Simulation Methods to the Transonic Potential Flow about Oscillating Wings," AIAA Paper 84-1564, June 1984; also, NLR MP 84057 U, May 1984.

[12]van der Vooren, J., van der Kolk, J.T., and Slooff, J. W., "A System for the Numerical Simulation of Sub- and Transonic Viscous Attached Flows around Wing-Body Configurations," AIAA Paper 82-0935, June 1982; also, NLR MP 82019 U, April 1982.

[13]Horsten, J. J., "Recent Developments in the Unsteady Pressure Measuring Technique at NLR," DGLR-Bericht 82-01, 1982, pp. 32-42; also, NLR MP 81055 U, Sept. 1981.

[14]Davis, S. S. and Malcolm, G. N., "Experiments in Unsteady Transonic Flow," AIAA Paper 79-769, April 1979.

[15]Houwink, R., "Some Remarks on Boundary Layer Effects on Unsteady Airloads," AGARD-CP-296, 1981, pp. 5-1 to 5-7.